Applied and Environmental Soil Science

WILEY

RESEARCH ARTICLE OPEN ACCESS

Spatial Assessment of Heavy Metal Contamination in Agricultural Soils of the Lower Chancay–Huaral Valley, Peru

Tomás Samaniego[1] | Jorge Ramirez[2] | Richard Solórzano[2,3]

[1]Dirección de Servicios Estratégicos Agrarios, Estación Experimental Agraria Donoso, Instituto Nacional de Innovación Agraria (INIA), Lima 15200, Peru | [2]Dirección de Servicios Estratégicos Agrarios, Centro Experimental la Molina, Instituto Nacional de Innovación Agraria—(INIA), Lima 15024, Peru | [3]Facultad de Ciencias Ambientales, Universidad Científica del Sur (UCSUR), Lima 15024, Peru

Correspondence: Richard Solórzano (investigacion_labsaf@inia.gob.pe)

Received: 12 January 2026 | **Revised:** 22 April 2026 | **Accepted:** 8 May 2026

Academic Editor: Kalyani Sen

Keywords: cadmium | environmental monitoring | kriging | soil contamination | spatial interpolation

ABSTRACT

Soil contamination by heavy metals (HMs) poses a potential threat to agricultural productivity and food security, particularly in rapidly developing coastal regions. This study evaluates the spatial distribution and contamination levels of cadmium (Cd), copper (Cu), lead (Pb), zinc (Zn), and manganese (Mn) in agricultural soils from the Huaral, Chancay, and Aucallama districts of the Lima region, Peru, an area undergoing urban expansion, mining concessions, and the establishment of a new international port. A total of 88 soil samples were analyzed for metal concentrations using microwave plasma atomic emission spectrophotometry (MP-AES), along with key physicochemical properties. Geostatistical interpolation techniques, including ordinary kriging (OK) and cokriging (CK), were applied to generate spatial prediction maps for each element. The geo-accumulation index (Igeo) and contamination factor (CF) were used to determine the contamination status. Mean Igeo values ranged from −0.59 to −0.46, while mean CF values ranged from 1.09 to 1.21, indicating generally unpolluted to moderately polluted conditions. Although maximum values reached 1.41 for Igeo and 4.21 for CF, these were spatially localized. Results revealed that most metal concentrations remained below the Peruvian Environmental Quality Standards for agricultural soils, suggesting predominantly natural geochemical origins. However, a small proportion of samples showed slight and localized exceedances (4.54% for Cd and 3.41% for Mn). For elements not regulated under national standards, international guidelines were considered, further supporting the absence of widespread anthropogenic contamination. Higher concentrations of Cd, Cu, Zn, Pb, and Mn were spatially clustered in the north-central sector of the study area, suggesting responses to soil properties such as pH, texture, and moisture. Notably, areas of higher concentration did not coincide with zones of higher contamination indices, indicating limited anthropogenic influence. However, proximity to urban expansion, mining activities, and port infrastructure highlights the need for continuous soil monitoring to prevent accumulation and ensure agricultural sustainability.

1 | Introduction

Soil and sediment geochemistry are critical to pinpointing the primary source of mineralization, soil origin, weathering conditions, and HM pollution [1–3]. In this context, soils are recognized as key environmental components that provide essential information on ecosystem conditions, acting both as carriers and potential sources of contaminants [4–6]. With the rapid development of the economy, mining, and human activities such as mineral resource exploitation, metal processing, smelting, chemical production, factory discharges, industrial and urban waste disposal, as well as agricultural practices and mining, the

concentrations of heavy metals (HMs) in soils have significantly increased [7–10]. Even at low concentrations, HMs can disrupt soil biochemical processes, inhibit microbial activity, and impair plant physiological functions, such as photosynthesis, gas exchange, and nutrient uptake, leading to reductions in crop yield and quality [11]. Beyond these well-known industrial and agricultural sources, HM contamination in urban–rural transition zones may also result from diffuse processes such as atmospheric deposition, irrigation with contaminated water, urban runoffs, fertilizers, pesticides, and waste incineration [12–14]. Therefore, distinguishing between natural background levels and anthropogenic inputs is a critical step toward ensuring soil quality, food safety, and sustainable agricultural development [15].

Currently, the traditional monitoring of soil HMs relies on chemical analysis methods, which provide high accuracy but are limited to small-scale applications. Large-scale monitoring of HM content, however, demands substantial human and material resources [16]. To better understand pollution dynamics, predicting the spatial distribution of HMs across broader areas is essential. Kriging has become one of the most widely applied geostatistical methods for this purpose, with ordinary kriging (OK) being recognized as the "best linear unbiased estimator" [12, 17]. While conventional kriging minimizes estimation error variance, it also produces a strong smoothing effect that may obscure areas of high spatial variability, causing values to converge toward the mean. Despite this limitation, kriging and its variants have been extensively applied to assess spatial heterogeneity, pollution sources, and contamination levels of HMs in soils across mining regions, metropolitan areas, and sensitive ecosystems [18].

However, spatially explicit assessments of HM contamination that integrate land use dynamics and proximity to anthropogenic sources remain scarce in Peruvian coastal valleys, despite the increasing environmental pressures associated with regional development. The study area encompasses the agricultural zones of Huaral, Chancay, and Aucallama, located in the Lima region of Peru. These districts are exposed to multiple potential sources of contamination, such as urban expansion, active mining concessions, and the recent construction of a large-capacity international port. Such activities have been widely recognized as drivers of soil pollution and the release of trace metals and organic compounds—particularly polycyclic aromatic hydrocarbons (PAHs)—in agricultural and peri-urban environments [19–21].

Therefore, this study aims to quantify and map the spatial distribution of five HMs (Cd, Cu, Pb, Zn, and Mn) in agricultural soils of the lower Chancay–Huaral Valley and to evaluate their contamination status and potential ecological risk using geoaccumulation and contamination factor (CF) indices. Geostatistical interpolation techniques—OK and cokriging (CK)—were applied to generate spatially continuous maps, enabling the identification of potential hotspots and assessing how soil physicochemical properties and proximity to anthropogenic activities influence metal accumulation patterns. This approach provides a baseline assessment in a rapidly transforming coastal region under increasing anthropogenic pressure, offering novel insights into the spatial variability of HMs and helping to distinguish between natural geochemical controls and potential early-stage anthropogenic impacts.

2 | Materials and Methods

2.1 | Study Area

The study was conducted in three districts (Huaral, Chancay, and Aucallama), located in the Lima region of Peru, within a subtropical desert ecosystem. The area is primarily used for agricultural production, with key crops including vegetables, fruit trees, and maize. Geographically, the study area is located between latitudes 11°40′ and 11°24′ S and longitudes 77°20′ and 77°04′ W, covering an estimated surface area of approximately 21790 ha (Figure 1). The study site is situated at elevations ranging from 0 to 354 m.a.s.l. Climatic records from the Huaral weather station report an average annual temperature of 20.3°C and a precipitation rate of 23.6 mm per year.

2.2 | Soil Sampling and Analysis

The sampling locations were determined using *R* software for Windows [22] through the *spsample* function of the "*sp*" package. A stratified sampling approach was applied using a Sentinel-2–derived raster layer to represent land-use variation across the study area. This method allowed the generation of 88 georeferenced sampling points distributed along the agricultural land-use gradient, ensuring adequate representation of cultivated soils while excluding nonagricultural zones. At each sampling point, a composite sample was obtained by collecting one central subsample and four additional subsamples at approximately 2 m in the cardinal directions. Soil samples were collected at two depths. For the topsoil layer (0–30 cm), five subsamples were extracted and thoroughly homogenized to produce a single composite sample. For the subsurface layer (30–60 cm), samples were collected by deepening the same pits used for the upper layer, ensuring that both depths corresponded to the same spatial location. This resulted in a total of 88 samples per depth. Approximately 1 kg of loose soil was collected from each depth, bagged, and stored in cool, dark conditions before transport to the laboratory. After air-drying, samples were sieved to 2 mm and analyzed for HM concentrations (Cd, Cu, Pb, Zn, and Mn) and physicochemical properties using the same procedures at INIA's Soil, Water, and Foliar Laboratories network. The evaluated variables formed part of a comprehensive soil characterization based on standardized reference methods. Soil texture (sand, silt, and clay percentages) was determined using the Bouyoucos hydrometer method [23]. The pH was measured following EPA guidelines [24], while electrical conductivity (EC) was determined using the saturation extract method (ISO, 11265) [25]. Soil organic carbon (SOC) was analyzed using NOM-021-RECNAT-2000 [23]. Available phosphorus for both neutral and acidic soils was measured using the Olsen method [23].

To determine the concentrations of Cd, Cu, Pb, Zn, and Mn, soil samples were digested according to the EPA Method 3050B [26]. One gram of sieved soil was treated with 10 mL of HNO_3 and left to react for 15 min at 95°C to facilitate digestion. Thereafter, we added 5 mL of concentrated HNO_3 and digested the sample for 30 min at a temperature of 95°C. Subsequently, 2 mL of deionized water and 3 mL of 30% H_2O_2 were added, and the mixture was digested for 2 h. Then, 10 mL of concentrated HCl was introduced, and the mixture was further digested for 15 min at 95°C. The extracts were diluted to 100 mL with deionized water and analyzed using a microwave plasma atomic emission

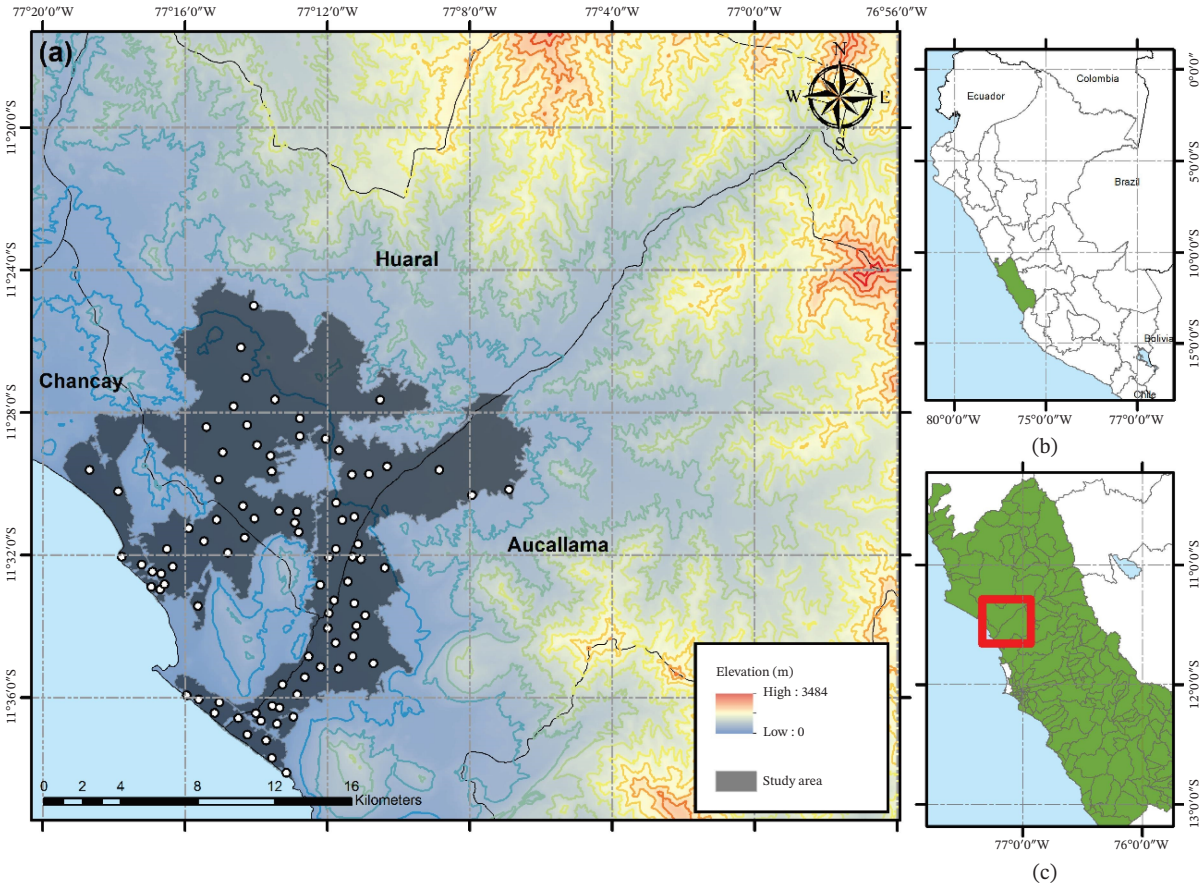

FIGURE 1 | Location of the study area in the districts of Chancay, Huaral, and Aucallama, Lima region, Peru. (a) Elevation map with sampling points; (b) location of the Lima region in Peru; and (c) study area within the Lima region.

spectrophotometer (MP-AES; Model 4210). Analyses were conducted following routine laboratory procedures, including instrument calibration and internal quality control practices, and analytical quality was supported through the use of certified multielement calibration standards (Agilent, Part No. 6610030000), ensuring traceability to international reference materials and calibration over an appropriate concentration range.

2.3 | HM Contamination assessment in Soil

CF [27] and geo-accumulation index (I_{geo}) [28] can be used to assess pollution, evaluate the pattern of contamination, and determine the potential risk due to exposure to ecological sensitivity, concentration, and toxicity of HMs in soil. The following equation estimated CF:

$$\mathrm{CF} = \frac{C_n}{C_b} \tag{1}$$

where C_n is the concentration of the element in the surface soil, and C_b is the geochemical background concentration. In this study, C_b values were derived from soil samples collected at depths of 30–60 cm, assuming minimal anthropogenic influence and representing local baseline conditions for the study area. I_{geo} was calculated by using the following formula:

$$I_{\mathrm{geo}} = \log_2\left(\frac{C_n}{1.5 * C_b}\right) \tag{2}$$

where C_n and C_b are as defined above. The factor 1.5 was used to account for natural variability in background concentrations due to lithogenic effects. The CF and I_{geo} index classifications for contamination levels are given in Table 1.

2.4 | Statistical Analysis

Correlation analysis was conducted to examine the relationships between soil HMs and edaphic properties, as well as the correspondence of each metal with its concentration at greater depths. All statistical analyses were performed in the *R* software for Windows [22] using the Hmisc and ggplot2 packages for computation and visualization. Prior to correlation analysis, the Shapiro–Wilk and Bartlett tests were applied to evaluate data normality and homogeneity of variances, respectively, in order to characterize the distributional properties of the dataset. Subsequently, pairwise correlations were calculated using Spearman's rank method, chosen for its robustness to nonparametric data distributions. The resulting correlation matrix was visualized through heatmaps with a diverging blue–white–red color scale, facilitating the interpretation of both the strength and significance of the associations among variables. Additionally, paired Wilcoxon signed-rank tests were performed to statistically compare HM concentrations between the two soil depths (0–30 cm and 30–60 cm). This nonparametric test was selected due to its suitability for data that deviate from normality. The results were further visualized using boxplots with significance letters to denote differences between depths.

TABLE 1 | Description of contamination factor and geo-accumulation index in soils [29].

Value	Sediments quality
Contamination factor	
$CF < 1$	Low contamination
$1 \leq CF < 3$	Moderate contamination
$3 \leq CF < 6$	Considerable contamination
$6 \leq CF$	Very high contamination
Geo-accumulation index	
$I_{geo} \leq 0$	Practically uncontaminated
$0 < I_{geo} < 1$	Uncontaminated to moderately contaminated
$1 < I_{geo} < 2$	Moderately contaminated
$2 < I_{geo} < 3$	Moderately to heavily contaminated
$3 < I_{geo} < 4$	Heavily contaminated
$4 < I_{geo} < 5$	Heavily to extremely contaminated
$5 < I_{geo}$	Extremely contaminated

2.5 | Interpolation Techniques

OK and CK were performed in RStudio using the packages gstat and automap, which allow flexible modeling of spatial dependence and automatic variogram fitting. OK is one of the most widely applied geostatistical techniques for spatial prediction, where the value at an unsampled location (X_0) is estimated as a weighted linear combination of neighboring observations [30]. The weights are derived from the spatial dependence structure represented by a fitted semivariogram model, ensuring unbiased predictions with minimum estimation variance [31].

CK extends the OK approach by incorporating one or more auxiliary variables that are spatially correlated with the target variable [32]. In this study, soil pH and the Normalized Difference Moisture Index (NDMI) were used as auxiliary variables, as they provide relevant information on soil chemical status and moisture conditions influencing the spatial distribution of heavy metals. The weights are determined according to the spatial structure of the variables and their cross-correlation, ensuring unbiased estimates with minimized variance. A fitted linear model of coregionalization is required to describe both the spatial continuity of the primary variable and its relationship with the auxiliary variables [33].

The predictive accuracy of the interpolation models was evaluated through cross-validation. In each iteration, one soil sample was removed and its concentration was estimated based on the remaining dataset. The comparison between observed and predicted values of Cd, Cu, Pb, Zn, and Mn allowed for assessing the model's performance. Three statistical indices were employed [34]:

$$R^2 = \frac{\sum_{i=1}^{n} (Zpi - Zoi)^2}{\sum_{i=1}^{n} (Zoi - Zo)^2} \quad (3)$$

$$\mathrm{RSME} = \sqrt{\frac{1}{n}\sum_{i=1}^{n} (Zpi - Zoi)^2} \quad (4)$$

$$\mathrm{MAE} = \frac{1}{n}\sum_{i=1}^{n} |Zpi - Zoi| \quad (5)$$

where n is the number of validation points, Zoi is the observed value at location i, Zpi is the predicted value, and $\overline{Z}\ o$ is the mean of observed values. The R^2 statistic quantifies the proportion of variance in the observations explained by the model, RMSE represents the average magnitude of prediction errors, and MAE measures the mean absolute deviation between predicted and observed values. Together, these indices provide a comprehensive assessment of model accuracy and its ability to reproduce the spatial distribution of HMs in soils.

3 | Results

3.1 | Statistical Summary of Soil Properties

The analyzed soil properties included organic carbon (OC), carbonate, particle size fractions (sand, silt, and clay), EC, P, bulk density (Bd), NDMI, and pH (see Table 2). OC content was generally low, ranging from 0.08% to 1.93%, with a mean of 0.59% and high variability (coefficient of variation [CV] = 61.60%). Its distribution was positively skewed (1.59), suggesting a predominance of soils with low OC and a few with higher levels. Carbonate content averaged 3.28%, with a broad range (0.52%–16.80%) and markedly high variability (CV = 104.62%), accompanied by strong positive skewness (2.10), reflecting the occurrence of extreme values. Sand was the dominant fraction, with values ranging from 45.29% to 91.02% (mean = 69.02%), exhibiting moderate variability (CV = 15.97%) and a near-symmetrical distribution (skewness = −0.18). Silt content ranged from 1.28% to 51.43%, with a mean of 18.00% and relatively high variability (CV = 45.25%), while clay ranged from 2.91% to 26.28% (mean = 13.00%), also showing considerable variability (CV = 43.82%). EC showed a wide dispersion, ranging from 0.03 to 39.49 $dS{\cdot}m^{-1}$, with a mean of 2.55 $dS{\cdot}m^{-1}$ and extremely high variability (CV = 187.03%), as well as strong positive skewness (6.01). Available phosphorus content varied between 5.95 and 24.72 $mg\ kg^{-1}$ (mean = 15.45 $mg{\cdot}kg^{-1}$), with moderate variability (CV = 29.09%) and a nearly symmetrical distribution (skewness = 0.07). Bd averaged 1.52 $g\ cm^{-3}$, with a narrow range (1.27–1.69 $g{\cdot}cm^{-3}$) and low variability (CV = 6.46%), indicating relatively homogeneous soil compaction conditions across the study area. NDMI values ranged from −0.53 to −0.11, with a mean of −0.28 and moderate variability (CV = 40.64%), showing a left-skewed distribution (skewness = −0.49). Finally, the soil pH was slightly acidic to neutral, ranging from 6.89 to 8.18, with an average of 7.59 and low variability (CV = 4.67%).

The Spearman correlation analysis revealed distinct associations between HM concentrations in the topsoil (0–30 cm) and selected soil parameters (Figure 2). Cd showed a significant negative correlation with soil pH ($r = -0.39$, $p < 0.05$) and with carbonate content ($r = -0.21$, $p < 0.05$), while being positively correlated with clay content ($r = 0.23$, $p < 0.05$). Cu exhibited a negative correlation with carbonate content ($r = -0.24$, $p < 0.05$) and a positive correlation with subsurface Cu concentrations (Cb; $r = 0.36$, $p < 0.05$). Zn was positively correlated with soil available P ($r = 0.27$, $p < 0.05$) and with subsurface Zn ($r = 0.41$, $p < 0.05$). Pb concentrations in the surface layer correlated positively with Pb in the subsurface ($r = 0.47$, $p < 0.05$). Similarly, Mn concentrations in the surface soil were positively correlated with subsurface Mn levels ($r = 0.47$, $p < 0.05$). These results highlight that both soil chemical properties (notably pH, P, and clay content)

TABLE 2 | Statistical characteristics of soil parameters.

	OC %	Carb %	Sand %	Silt %	Clay %	EC $DS{\cdot}m^{-1}$	P $mg{\cdot}kg^{-1}$	Bd $g{\cdot}cm^{-3}$	NDMI —	pH —
Min	0.08	0.52	45.29	1.28	2.91	0.03	5.95	1.27	−0.53	6.89
Max	1.93	16.80	91.02	51.43	26.28	39.49	24.72	1.69	−0.11	8.18
Mean	0.59	3.28	69.02	18.00	13.00	2.55	15.45	1.52	0.28	7.59
Median	0.49	1.84	71.12	16.68	12.00	1.43	15.64	1.54	−0.26	7.60
Std. deviation	0.37	3.43	11.02	8.14	5.70	4.76	4.49	0.10	0.11	0.35
CV	61.60	104.62	15.97	45.25	43.82	187.03	29.09	6.46	40.64	4.67
Kurtosis	2.82	4.33	−0.73	2.58	−0.53	42.91	−0.35	−0.45	−0.75	−0.95
Skewness	1.59	2.10	−0.18	1.07	0.42	6.01	0.07	−0.52	−0.49	−0.19

and subsurface metal concentrations exert significant influences on the distribution of HMs in surface soils.

The concentration of HMs in the soil profile (0–30 cm and 30–60 cm) is summarized in Table 3. Cd content ranged from 0.25 to 1.50 $mg{\cdot}kg^{-1}$ in the surface layer and from 0.25 to 1.24 $mg{\cdot}kg^{-1}$ in the subsurface, with similar mean values of 0.87 and 0.86 $mg{\cdot}kg^{-1}$, respectively. Variability was moderate (CV = 31.59% and 25.36%), and the distribution was approximately symmetrical in the surface horizon (skewness = 0.06) but negatively skewed in the subsurface (−1.30). Cu concentrations showed a broader range, from 33.21 to 120.73 $mg{\cdot}kg^{-1}$ at 0–30 cm and from 32.82 to 139.85 $mg{\cdot}kg^{-1}$ at 30–60 cm, with mean values of 72.11 and 67.20 $mg{\cdot}kg^{-1}$, respectively. Variability was moderate to high (CV = 25.74%–31.26%), and both layers exhibited positive skewness (0.52 and 0.97), indicating the presence of higher-than-average values in some samples. Pb levels averaged 22.40 $mg{\cdot}kg^{-1}$ in the surface and 21.44 $mg{\cdot}kg^{-1}$ in the subsurface, with moderate variability (CV = 36.90% and 44.20%). The distributions were positively skewed (0.36 and 0.78), reflecting occasional elevated concentrations. Mn exhibited the highest concentrations among the analyzed elements, ranging from 201.00 to 958.70 $mg{\cdot}kg^{-1}$ in the surface horizon and from 215.74 to 929.69 $mg{\cdot}kg^{-1}$ in the subsurface, with mean values of 469.45 and 450.28 $mg{\cdot}kg^{-1}$, respectively. Variability was high (CV = 34.65%–31.40%), and distributions showed positive skewness (1.07 and 0.82), suggesting that extreme values strongly influenced the mean. Zn concentrations ranged from 4.98 to 63.70 $mg{\cdot}kg^{-1}$ at 0–30 cm and from 9.99 to 77.14 $mg{\cdot}kg^{-1}$ at 30–60 cm, with mean values of 26.84 and 25.76 $mg{\cdot}kg^{-1}$. Variability was considerable (CV = 42.65% and 51.91%), and distributions were positively skewed (1.04 and 2.06), particularly in the subsurface layer, as confirmed by a light-tailed distribution (kurtosis = 5.14).

The Wilcoxon test was applied to compare HM concentrations between soil depths (0–30 cm and 30–60 cm) (Figure 3). No significant differences were observed for Cd, Cu, Pb, and Mn ($p > 0.05$), indicating a relatively uniform distribution across depths. In contrast, Zn showed a significant difference ($p < 0.05$), with higher concentrations in the 0–30-cm layer compared to the 30–60-cm layer. These results suggest that, except for Zn, the vertical distribution of HMs in the study area is relatively homogeneous.

The CF of the analyzed HMs ranged from 0.19 for Cu to 4.21 for the same element, with mean values close to 1.0 for all metals, indicating generally low levels of contamination (Table 4). Cd

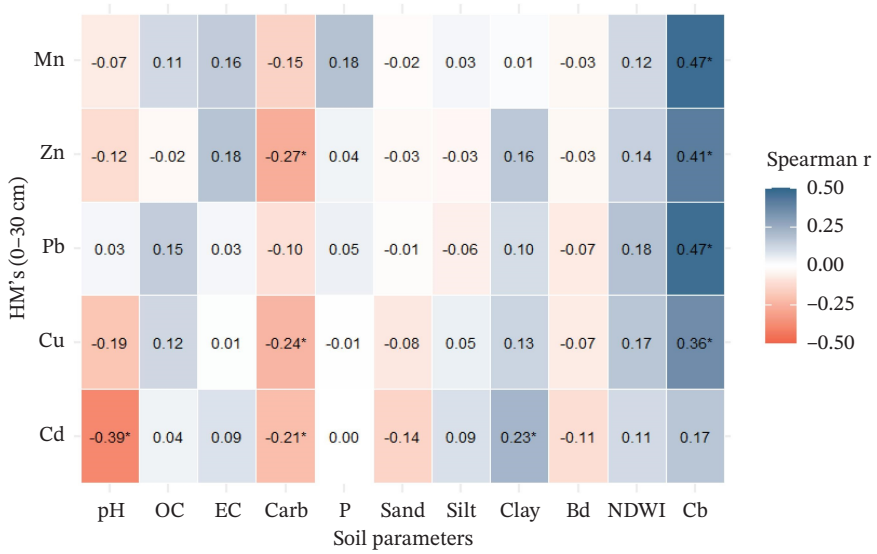

FIGURE 2 | Heatmap showing Spearman correlation coefficients between heavy metal concentrations in the surface soil layer (0–30 cm) and selected soil parameters. Significant correlations ($p < 0.05$) are marked with an asterisk.

TABLE 3 | Statistical characteristics of soil HMs.

	Cd (mg·kg^{-1})		Cu (mg·kg^{-1})		Pb (mg·kg^{-1})		Mn (mg·kg^{-1})		Zn (mg·kg^{-1})	
	0–30	30–60	0–30	30–60	0–30	30–60	0–30	30–60	0–30	30–60
LOQ	0.18		1.24		0.15		2.36		1.67	
Min	0.25	0.25	33.21	32.82	5.39	6.31	201.00	215.74	4.98	9.99
Max	1.50	1.24	120.73	139.85	41.69	47.55	958.70	929.69	63.70	77.14
Mean	0.87	0.86	72.11	67.20	22.40	21.44	469.45	450.28	26.84	25.76
Median	0.85	0.87	69.36	64.37	21.18	19.89	427.57	411.89	24.94	22.96
Std. deviation	0.27	0.22	18.56	21.01	8.27	9.48	162.66	141.37	11.45	13.37
CV	31.59	25.36	25.74	31.26	36.90	44.20	34.65	31.40	42.65	51.91
Kurtosis	0.21	2.17	0.05	1.26	−0.34	0.20	1.03	0.59	1.39	5.14
Skewness	0.06	−1.30	0.52	0.97	0.36	0.78	1.07	0.82	1.04	2.06
References										
Ccopi et al. [35]	0.38–4.86		26.5–278		22.9–501		745–1746		88.3–2413	
Alejos-Patiño et al. [36]	0.18		15.74		32.39		392		81	
Tarrillo et al. [37]	1.1 2.0		7–60		4–24		240–1099		22–110	
Santos-Francés et al. [38]	2.14–2.43		1.90–35.80		11.60–170.70		—		26.80–80.20	
Orellana-Mendoza et al. [39]	0.12–0.40		—		4.67–67.82		—		36.55–124.18	

presented CF values between 0.21 and 4.00, with a mean of 1.12 (CV = 55.8%), while Pb varied from 0.28 to 2.83, with an average of 1.16 (CV = 42.5%). Similarly, Zn and Mn showed CF ranges of 0.48–2.69 and 0.38–2.46, with mean values of 1.14 and 1.09, respectively. Regarding the I_{geo} values, they were consistently negative on average, with means ranging from −0.46 (Zn) to −0.59 (Cd), suggesting no contamination (Table 4). Minimum I_{geo} values reached −2.99 for Cu and −2.84 for Cd, while maximum values did not exceed 1.49 (Cu). Notably, the variability of I_{geo} was high across all metals, with a CV exceeding 88%, particularly for Cu (CV = 152.1%). The distributions of CF were positively skewed, particularly for Cd (skewness = 2.34) and Cu (skewness = 1.92), indicating the presence of localized sites with elevated concentrations.

3.2 | Spatial Mapping of HMs

The spatial distribution of CF values for Cd, Cu, Pb, Zn, and Mn is presented in Figure 4. Overall, the point patterns showed broad similarities among metals, although localized differences were evident. For Cd (Figure 4a), CF values < 1 were widely distributed across the study area, together with values between 1 and 2, whereas the highest values (> 2) were concentrated in the southern zones of the study area. A similar pattern was observed for Cu (Figure 4b), where CF values < 1 showed no clear spatial trend, similar to values between 1 and 2, although the latter were predominantly concentrated in the southern part of the study area. In contrast, values > 2 were scarce and scattered across different locations, without indicating any marked spatial tendency. For Pb (Figure 4c), CF values < 1 showed no clear spatial trend, similar to values between 1 and 2, although the latter were predominantly concentrated in the central part of the study area. In contrast, most of the values > 2 were clustered in the north-central sector, with no sites exceeding a CF of 3. For Zn (Figure 4d), CF values < 1 showed no clear spatial trend, similar to values between 1 and 2, although the latter were predominantly concentrated in the southern part of the study area. Values between 2 and 3 were scarce and scattered across different locations, while no sites recorded CF values above 3. Mn (Figure 4e) displayed a more homogeneous spatial distribution, with the majority of sites falling within low to moderate CF ranges (< 2.0). Collectively, these results indicate that although contamination is generally low to moderate across the region, specific sites exhibit elevated CF values that may warrant further monitoring.

The spatial distribution of I_{geo} values for Cd, Cu, Pb, Zn, and Mn is presented in Figure 5. Overall, the point patterns revealed generally low levels of accumulation across the study area, although localized differences in metal concentrations were evident. For Cd (Figure 5a), I_{geo} values below −1 were widespread throughout the region, together with values ranging from −1 to 0, whereas the highest values (> 1.0) were mainly concentrated in the southeastern sector. For Cu (Figure 5b), I_{geo} values < −1 and those between −1 and 0 showed no clear spatial trend, while values between 0 and 1 were mostly concentrated in the southern part of the study area. A few sites exceeded $I_{geo} > 1$, but these were isolated and did not define a clear pattern. For Pb (Figure 5c), I_{geo} values between −1 and 0 predominated across most of the area, while higher values (0–1) were mainly clustered in the north-central and southern parts of the study area. In this case, no sampling points showed $I_{geo} > 1$. For Zn (Figure 5d), I_{geo} values < 0 dominated the study area, while values between 0 and 1 were dispersed across different locations. No points exceeded $I_{geo} = 1$. Mn (Figure 5e) exhibited a homogeneous distribution, with most of the sampling points falling within negative I_{geo} values. Points with I_{geo} values between 0 and 1 were mainly located in the north-central sector of the study area, and no sites recorded values above 1. Collectively, these results indicate that HM accumulation in soils is generally low across the study area, with only localized and moderate enrichment in specific sites, possibly associated with natural processes including weathering of rocks and minerals, erosion, and atmospheric deposition.

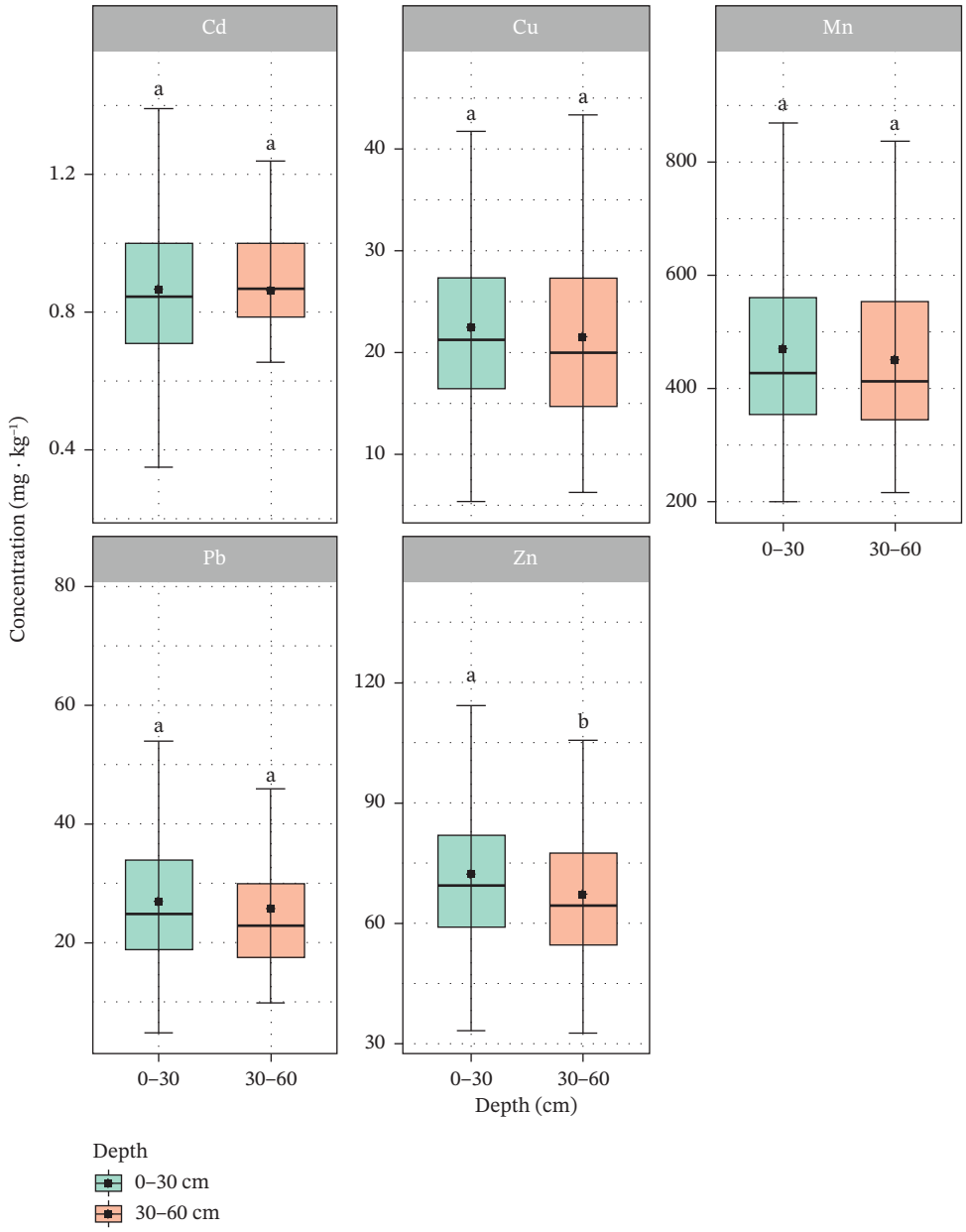

FIGURE 3 | Boxplots showing the distribution of Cd, Cu, Mn, Pb, and Zn concentrations at two soil depths (0–30 cm and 30–60 cm). Statistical differences between depths were evaluated using the Wilcoxon test; different lowercase letters indicate significant differences ($p < 0.05$).

TABLE 4 | Statistical characteristics of the contamination index.

	Cd		Cu		Pb		Zn		Mn	
	CF	I_{geo}	**CF**	I_{geo}	**CF**	I_{geo}	**CF**	I_{geo}	**CF**	I_{geo}
Min	0.21	−2.84	0.19	−2.99	0.28	−2.44	0.48	−1.63	0.38	−1.97
Max	4.00	1.41	4.21	1.49	2.83	0.92	2.69	0.84	2.46	0.72
Mean	1.12	−0.59	1.21	−0.49	1.16	−0.50	1.14	−0.46	1.09	−0.54
Median	0.98	−0.61	1.11	−0.43	1.08	−0.47	1.09	−0.46	1.05	−0.52
Std. deviation	0.63	0.71	0.64	0.75	0.50	0.67	0.38	0.45	0.36	0.48
CV	55.80	119.67	52.53	152.14	42.52	133.65	33.31	98.33	33.38	88.74
Kurtosis	7.04	2.09	6.15	1.54	0.81	0.49	3.26	0.57	1.94	0.71
Skewness	2.34	−0.12	1.92	−0.52	0.73	−0.64	1.39	0.15	1.01	−0.23

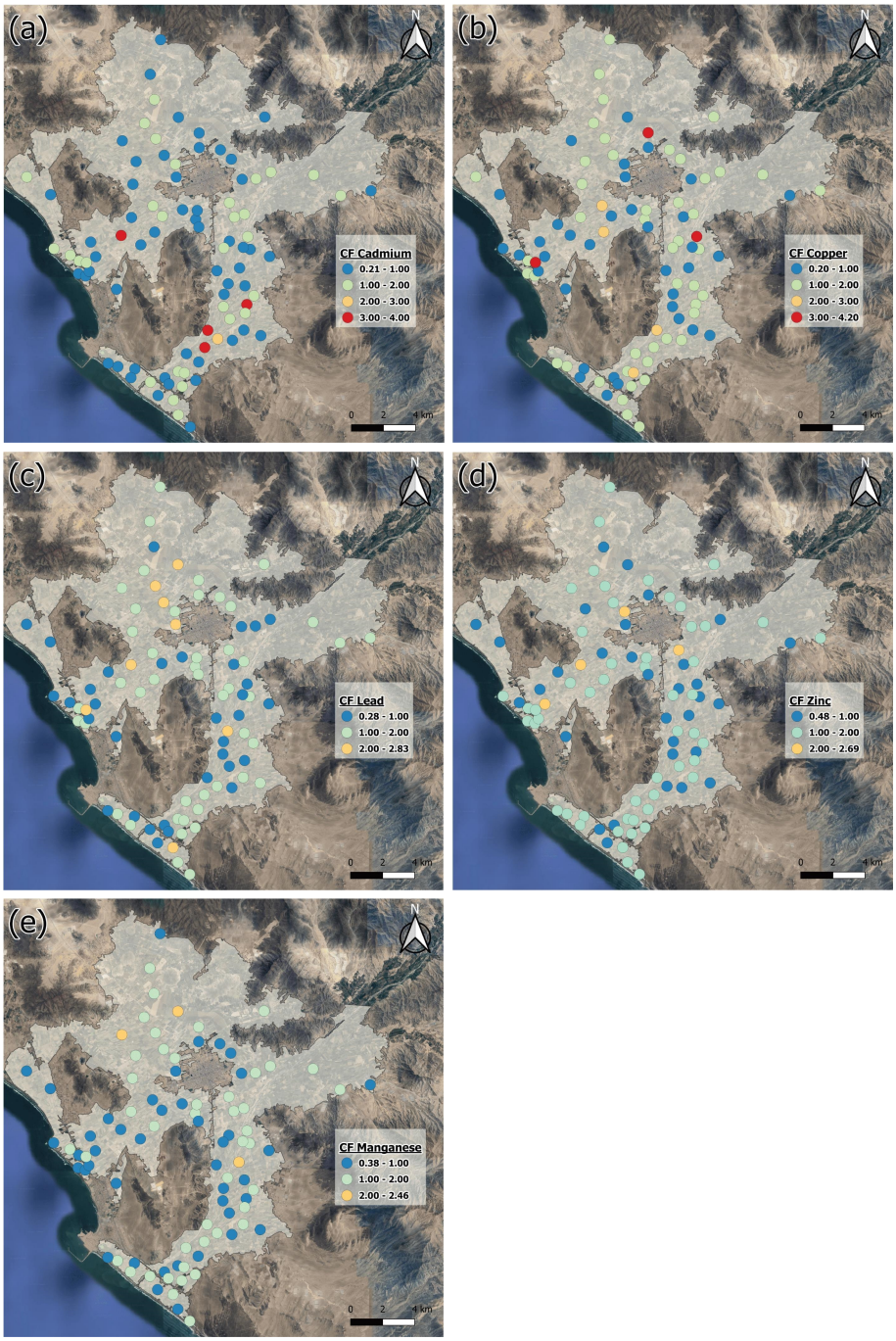

FIGURE 4 | Spatial distribution of CF values for HMs across 88 sampling points: (a) Cd, (b) Cu, (c) Pb, (d) Zn, and (e) Mn.

The performance of the OK and CK models for Cd, Cu, Pb, Zn, and Mn was assessed using five statistical indicators (Table 5). Among the analyzed metals, Cu showed the best predictive performance, with the highest coefficient of determination ($R^2 = 0.62$), the lowest mean absolute error (MAE = 0.71), and the smallest CV_RMSE (22.81), indicating a relatively strong model fit and consistent predictions. Pb exhibited intermediate performance, with an R^2 of 0.50 but a higher RMSE (8.04) and CV_RMSE (29.97), reflecting moderate predictive reliability. Cd, Zn, and Mn showed comparatively lower accuracy, with R^2 values around 0.42–0.43 and higher CV_RMSE values (> 23), suggesting greater variability and less precise estimations. Despite these differences, all models achieved acceptable levels of predictive performance, capturing the general spatial variability of HM concentrations across the study area.

The spatial interpolation maps of HM concentrations (Cd, Cu, Pb, Zn, and Mn) across the study area are presented in Figure 6. These maps illustrate the predicted spatial distribution patterns obtained from the geostatistical interpolation of measured values. Overall, the concentration patterns vary among metals, yet some shared spatial tendencies can be observed. Cd (Figure 6a) shows elevated concentrations mainly in the southeastern and north-central parts of the study area, while lower values dominate the western sector near the coast. Cu (Figure 6b) exhibits a similar spatial configuration, with higher

FIGURE 5 | Spatial distribution of I_{geo} values for HMs across 88 sampling points: (a) Cd, (b) Cu, (c) Pb, (d) Zn, and (e) Mn.

TABLE 5 | Performance metrics of OK and CK models.

Metals	Model	Variogram model	R^2	RMSE	MAE	AIC	CV_RMSE
Cd	CK	Spherical	0.42	0.21	0.78	−265.00	23.94
Cu	CK	Stein model	0.62	5.11	0.71	299.10	22.81
Pb	OK	Stein model	0.50	8.04	0.70	372.95	29.97
Zn	CK	Spherical	0.42	14.17	0.73	478.62	19.65
Mn	OK	Stein model	0.43	120.48	0.74	852.21	26.09

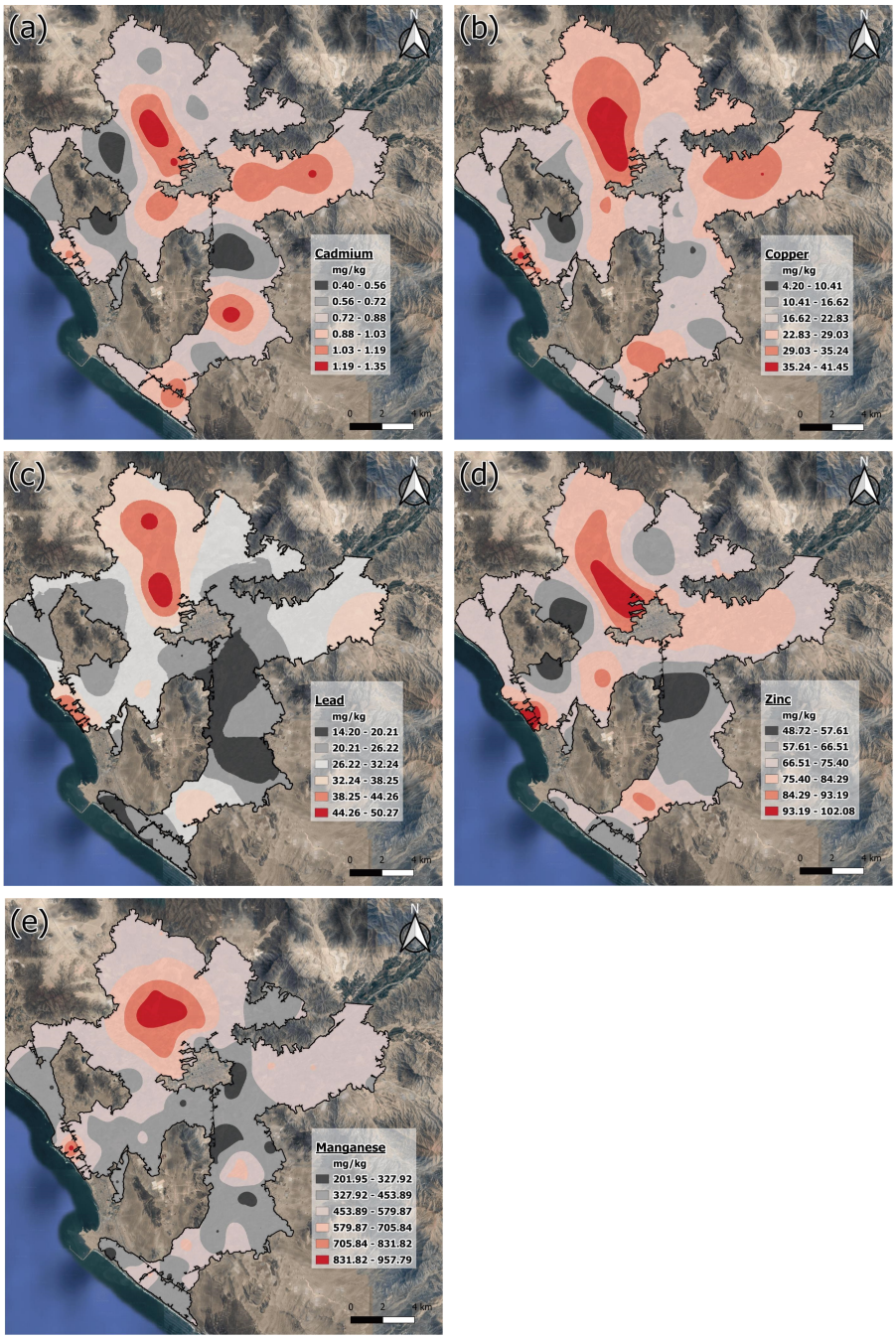

FIGURE 6 | Spatial distribution maps of HMs generated using OK and CK: (a) Cd, (b) Cu, (c) Pb, (d) Zn, and (e) Mn. The color gradients represent metal concentrations, where dark gray indicates areas of lower concentration and red denotes zones of higher concentration.

concentrations in the north-central and coastal zones, gradually decreasing toward the south. Pb (Figure 6c) presents a distinct pattern, with the highest concentrations concentrated in the north-central area, while lower values prevail in the southern and coastal regions. In the case of Zn (Figure 6d), the highest values are also found in the north-central and southwestern areas, demonstrating spatial consistency with the distributions of Cu and Pb. Finally, Mn (Figure 6e) exhibits its highest concentrations in the north-central portion of the study area, with a decreasing trend toward the southern and coastal zones. Collectively, these spatial patterns suggest that the central and northern parts of the region exhibit localized enrichment of HMs, potentially influenced by both natural soil properties and anthropogenic inputs such as fertilizers, pesticides, wastewater irrigation, and agricultural and urban runoffs, while the southern and coastal zones remain comparatively less affected.

4 | Discussion

4.1 | Relationships Between Soil Properties and HMs

The correlation matrix (Figure 2) reveals distinct relationships between HM concentrations in the surface layer (0–30 cm) and key soil properties. Among these, pH and carbonate content exhibited the most consistent inverse correlations with HM

concentrations, with the latter showing a significant negative relationship with Cd, Zn, and Cu. This pattern suggests that soils with higher carbonate content tend to immobilize these metals, reducing their solubility and bioavailability. The negative association between pH and metal concentrations aligns with the effect of soil alkalinity on metal speciation: As pH increases, metals such as Cd^{2+} and Cu^{2+} tend to form less soluble hydroxides or carbonates, leading to greater adsorption onto mineral surfaces [40, 41]. Likewise, the low content of humic substances limits the formation of soluble organometallic complexes, thereby reducing the solubility and bioavailability of HMs [42]. This buffering effect is particularly relevant in semiarid soils, where pH values typically remain above neutral and carbonate accumulation is common, effectively restricting metal mobility [43, 44]. The significant inverse correlation between Cd and carbonate content underscores the strong affinity of Cd for carbonate minerals, a mechanism that has been reported in calcareous soils where Cd coprecipitates with $CaCO_3$ or is retained on carbonate surfaces [45, 46]. Similarly, Cu showed moderate negative correlations with both pH and carbonates, reflecting its tendency to form stable complexes with carbonate and hydroxyl groups [47]. In contrast, Mn showed no significant correlations with the evaluated soil properties, consistent with the findings of Obasi et al. [48]. However, other studies have reported significant associations of Mn with clay minerals, H_2O, and OH^- groups [49]. A similar pattern was observed for Pb, which appears to be more closely influenced by clay mineralogy and humified organic matter [50, 51]. Nevertheless, in the present study, Pb did not show significant relationships with either clay content or soil organic matter. Overall, these relationships underscore the significance of soil pH and carbonate buffering capacity in regulating HM availability in the study area.

The predominance of neutral to slightly alkaline conditions appears to favor metal immobilization, contributing to the low environmental risk observed in the contamination assessment. The concentrations of HMs observed in both soil layers remained generally below the threshold limits established by the Peruvian Environmental Quality Standards for soil [52]. According to these guidelines, the permissible levels for agricultural soils are 1.4 mg kg^{-1} for Cd, 140 mg kg^{-1} for Cu, and 70 mg kg^{-1} for Pb. Most measured concentrations in the present study were lower than these reference values, indicating an overall low degree of contamination and limited anthropogenic enrichment. However, a small proportion of samples slightly exceeded the threshold value for Cd, while Cu concentrations approached but did not exceed the regulatory limit. For Zn, which is not regulated under the Peruvian ECA, international guidelines were used for comparison. The Canadian Soil Quality Guideline [53] establishes a threshold of 250 mg kg^{-1} for agricultural soils. All Zn concentrations in this study were well below this value, indicating no risk associated with this element. For Mn, which is also not regulated under the Peruvian ECA, international benchmarks were considered. The U.S. EPA Ecological Soil Screening Level [54] establishes a threshold of approximately 900 mg kg^{-1} for Mn in agricultural soils. Although most Mn concentrations were below this limit, the highest values slightly exceeded this benchmark, suggesting localized enrichment that may be related to natural soil-forming processes rather than anthropogenic inputs.

The behavior of metals along the soil profile can vary depending on multiple factors, including the degree and nature of contamination, soil physicochemical characteristics, and environmental conditions. In some cases, higher concentrations may occur in deeper layers due to leaching or past contamination events [55], while in others, surface enrichment is more evident as a result of recent deposition or anthropogenic inputs [56–58]. In this study, however, no significant differences were observed between the two evaluated depths, consistent with the findings reported by Mitran et al. [42], who also found no significant variations in metal concentrations with soil depth, indicating a relatively uniform vertical distribution within the profile.

4.2 | Spatial Patterns and Modeling Performance of Heavy Metals

Table 4 presents the descriptive statistics of the CF and the I_{geo} for Cd, Cu, Pb, Zn, and Mn. Overall, the mean CF values (< 1.5) and negative I_{geo} values indicate that most sampling points correspond to uncontaminated or low-contamination levels [59–62]. The median CF values approximating unity and the consistently negative I_{geo} values suggest that the observed metal concentrations are largely controlled by natural geochemical background levels, with limited evidence of significant anthropogenic influence. Similar trends of low CF and I_{geo} values have been reported in other agricultural and mountainous soils, suggesting minimal contamination and predominantly lithogenic control of metal contents [29, 63, 64]. Many studies reporting high CF and I_{geo} values tend to occur in areas with acidic soils and heavy anthropogenic inputs (e.g., mining-influenced zones), where acid pH and abundant soil moisture promote metal mobility [38, 65, 66]. However, investigations have also found no zones of high contamination in similarly acidic soils [67, 68]. Conversely, some studies highlight elevated contamination even in alkaline or neutral soils when metal inputs are high or soil buffering is overwhelmed [37]. The findings show that, although localized hotspots with elevated CF and I_{geo} values were identified (Figures 4 and 5), the majority of sampling points fall within the low-contamination category. This suggests that soil physicochemical properties—particularly pH, clay content, and organic matter—play a predominant role in limiting metal availability and accumulation [66]. This occurs despite the fact that the study area encompasses the urban centers of Huaral and Chancay, whose populations were estimated at around 112,000 and 65,000 inhabitants, respectively, in 2024 (INEI, 2017), and also includes a mining concession (Colquisiri S.A.) that produces Cu, Zn, Ag, and Pb. Therefore, the generally low contamination indices do not reflect a lack of potential pollution sources but rather the strong buffering and retention capacity of the local soils, which is consistent with findings reported by Tiabou et al. previous studies [14, 70].

The model's performance metrics, summarized in Table 5, indicate moderate predictive accuracy across the analyzed metals, with R^2 values ranging from 0.42 to 0.62. This variability suggests that interpolation performance is governed not only by the statistical distribution of each variable but also by the strength of spatial autocorrelation and the suitability of auxiliary covariates [71]. The highest performance was observed for Cu ($R^2 = 0.62$), where CK with NDMI effectively captured spatial dependencies related to soil moisture and vegetation cover, improving spatial prediction accuracy. In contrast, Cd (cokriged with pH) and Zn (cokriged with NDMI) exhibited lower determination

coefficients ($R^2 = 0.42$) and higher relative errors, indicating that their spatial variability was only partially explained by the auxiliary variables. For Pb and Mn, modeled using OK, intermediate R^2 values (0.43–0.50) and higher AIC scores suggest limited spatial structure or more localized variability. Overall, both OK and CK effectively captured the spatial variability of metal concentrations, with CK (for Cd, Cu, and Zn) maintaining spatial coherence by integrating auxiliary covariates linked to soil chemistry and hydrological conditions. Meanwhile, Pb and Mn were adequately represented through OK, reflecting their intrinsic spatial autocorrelation. These results are consistent with previous studies highlighting the benefit of incorporating environmental covariates—such as pH, OC, and moisture indices—to enhance the spatial representativeness of geostatistical models [72–74]. Spatially, the interpolated maps (Figure 6) reveal that the highest concentrations of Cd, Cu, Zn, Pb, and Mn tend to cluster in the north-central portion of the study area, suggesting that these elements respond similarly to underlying soil properties and environmental conditions. This spatial coincidence likely reflects shared soil attributes—such as pH, texture, and moisture retention—that regulate metal mobility and adsorption processes. Consistently, Yangtao et al. [75] reported similar spatial distribution patterns for these same metals, indicating common controlling mechanisms.

4.3 | Implications for Soil Management

The areas of higher metal concentration do not coincide with the locations showing the highest contamination indices (Figures 4 and 5), implying that these zones are not currently subject to active anthropogenic pollution. Nonetheless, given their proximity to urban and industrial activities, these areas warrant continuous monitoring to prevent future increases in metal levels that could surpass regulatory thresholds. Moreover, in these zones with higher concentrations, it is advisable to implement management practices that minimize conditions favoring metal mobilization and bioavailability, such as maintaining a neutral to slightly alkaline soil pH, improving organic matter content, and avoiding excessive irrigation or the use of acidifying fertilizers. Additional remediation strategies may include the application of organic amendments [76] and mineral amendments such as tourmaline [77], which enhance metal immobilization through adsorption and complexation processes. Studies have also demonstrated that certain microorganisms, such as *Aspergillus* species, can promote the immobilization of heavy metals via the production of organic acids [78]. Conventional approaches, such as phytoremediation using plant species with strong metal uptake capacity [79], may also be effective. In the long term, the development and use of rootstocks tolerant to or selective for heavy metals, as recently explored in crops such as tomato and grapevine [80, 81], should be promoted as part of a sustainable soil management strategy. Similar precautionary approaches have been recommended in agricultural and peri-urban soils where the soil system's protective capacity against HM accumulation is inherently limited [82].

5 | Conclusions

This study provides an integrated assessment of the spatial distribution and contamination status of Cd, Cu, Pb, Zn, and Mn in agricultural soils from the Huaral, Chancay, and Aucallama districts in central Peru. The results indicate that the concentrations of the analyzed metals generally remain below the permissible limits established by the Peruvian Environmental Quality Standards for soils, suggesting a predominance of natural geochemical contributions with limited evidence of anthropogenic influence. Nonetheless, a small proportion of samples slightly exceeded the threshold values (4.54% for Cd and 3.41% for Mn), although these exceedances were marginal and spatially localized, and may be associated with natural variability rather than widespread anthropogenic contamination. Geostatistical interpolation using OK and CK effectively captured the spatial variability of metal concentrations, revealing zones with relatively higher accumulation in the north-central portion of the study area. These spatial patterns appear to be governed by shared soil properties and environmental factors, such as pH, texture, and moisture retention, rather than by direct anthropogenic inputs. However, given the proximity of the study area to expanding urban zones, mining concessions, and the newly developed international port, continuous soil monitoring is recommended to ensure that current concentrations remain stable and do not evolve into potential contamination risks for local agricultural systems.

Funding

This research was funded by the INIA project "Mejoramiento de los servicios de investi-gación y transferencia tecnológica en el manejo y recuperación de suelos agrícolas degradados y aguas para riego en la pequeña y mediana agricultura en los departamentos de Lima, Áncash, San Martín, Cajamarca, Lambayeque, Junín, Ayacucho, Arequipa, Puno y Ucayali" CUI 2487112.

Conflicts of Interest

The authors declare no conflicts of interest.

Data Availability Statement

The data that support the findings of this study are available from the corresponding author upon reasonable request.

References

1. L. P. Yiika, A. R. Meniemoh, E. E. Mengu, C. T. Berinyuy, K. Nono, and G. Djibril, "Geochemistry and Source Area Weathering of Soils Around Mount Bamboutos (Cameroon Volcanic Line)," *Advances in Analytic Science* 6, no. 1 (2025): 3670, https://doi.org/10.54517/AAS3670.

2. A. A. Ngambu, B. K. Fomekong, S. M. Chofor, et al., "Geochemical and Petrographic Characterization of Heavy Mineral Fractions in Stream Sediments From Akum Area, Northwest Cameroon: Implications for Sources, Weathering and Mineral Exploration," *Journal of the Cameroon Academy of Sciences* 22, no. 2 (2025): 181–199, https://doi.org/10.4314/JCAS.V22I2.6.

3. N. M. Jean-Lavenir, S. Cyrille, E. D. Omar, L. P. Yiika, and E. E. M. Junior, "Geochemical and Gold-Ore Potential Assessment in Stream Sediments of Bindiba Gold District, Eastern Cameroon: Implications for Gold Exploration, Sediment Provenance, Paleoenvironment, and Tectonic Setting," *Mining, Metallurgy & Exploration* 42, no. 4 (2025): 2415–2439, https://doi.org/10.1007/S42461-025-01270-9.

4. G. C. Suh, N. A. Afahnwie, A. F. Tiabou, K. N. G. Djibril, A. R. Meniemoh, and L. P. Yiika, "Source Apportionment, Ecological and Toxicological Risk Assessment of Trace Metals in Agricultural Soils of Wabane, South West Region, Cameroon," *Journal of Trace Elements and Minerals* 12 (2025): 100218, https://doi.org/10.1016/J.JTEMIN.2025.100218.

5. A. F. Tiabou, C. N. Esuka, I. F. Mbowou Ngantche, L. P. Yiika, B. P. Wadgua, and C. M. Agyingi, "Spatial Distribution, Contamination Characteristics and Eco-Risk Assessment of Toxic Metals in Stream Sediments of Njombe-Penja Banana Plain, Cameroon Volcanic Line," *Chemistry Africa* 8, no. 2 (2024): 619–639, https://doi.org/10.1007/S42250-024-01159-Y.

6. N. M. Jean-Lavenir, T. N. Kiki, L. P. Yiika, and G. M. Ndi, "Contamination, Sources and Risk Assessments of Metals in Stream Sediments of Pouma Area, Pan-African Fold Belt, Southern Cameroon," *Water, Air, & Soil Pollution* 234, no. 3 (2023): 160, https://doi.org/10.1007/S11270-023-06180-4.

7. X. Xu, Y. Zhao, X. Zhao, Y. Wang, and W. Deng, "Sources of Heavy Metal Pollution in Agricultural Soils of a Rapidly Industrializing Area in the Yangtze Delta of China," *Ecotoxicology and Environmental Safety* 108 (2014): 161–167, https://doi.org/10.1016/J.ECOENV.2014.07.001.

8. D. Gasparatos, "Soil Contamination by Heavy Metals and Metalloids," *Environments* 9, no. 3 (2022): 32–39, https://doi.org/10.3390/ENVIRONMENTS9030032.

9. L. P. Yiika, N. M. Jean-Lavenir, M. G. M. MonespÃ©rance, E. E. Mengu, and B. E. Bih, "Contamination and Risk Assessment of Heavy Metals in Stream Sediments of Bambui Area, Western Cameroon," *International Journal of Research and Innovation in Applied Science* 7 (2022): 64–75.

10. C. Sigué, N. E. Yewong, L. P. Yiika, et al., "Assessment of Contamination, Sources and Health Risks of Potentially Hazardous Elements in Surface Sediments of Dibang, Cameroon," *Discover Environment* 3, no. 1 (2025): 165, https://doi.org/10.1007/S44274-025-00363-Y.

11. E. Orellana-Mendoza, V. Camel, L. Yallico, V. Quispe-Coquil, and R. Cosme, "Effect of Fertilization on the Accumulation and Health Risk for Heavy Metals in Native Andean Potatoes in the Highlands of Perú," *Toxicology Reports* 12 (2024): 594–606, https://doi.org/10.1016/J.TOXREP.2024.05.006.

12. J. Zhou, K. Feng, Y. Li, and Y. Zhou, "Factorial Kriging Analysis and Sources of Heavy Metals in Soils of Different Land-Use Types in the Yangtze River Delta of Eastern China," *Environmental Science and Pollution Research* 23, no. 15 (2016): 14957–14967, https://doi.org/10.1007/S11356-016-6619-Z/METRICS.

13. H. Sanad, R. Moussadek, L. Mouhir, M. O. Lhaj, H. Dakak, and A. Zouahri, "Geospatial Analysis of Trace Metal Pollution and Ecological Risks in River Sediments From Agrochemical Sources in Morocco's Sebou Basin," *Scientific Reports* 15, no. 1 (2025): 16701, https://doi.org/10.1038/s41598-025-01199-5.

14. A. F. Tiabou, G. M. M. Mboudou, M. M. Ghanyuymo, L. P. Yiika, and N. E. Forchenallah, "Evaluation of Surface and Groundwater Quality in Logbadjeck Quarrying Area: Implications for Trace Metals Pollution and Health Risk Assessment," *International Journal of Energy and Water Resources* 9, no. 2 (2024): 893–915, https://doi.org/10.1007/S42108-024-00321-Z.

15. P. K. Rai, S. S. Lee, M. Zhang, Y. F. Tsang, and K. H. Kim, "Heavy Metals in Food Crops: Health Risks, Fate, Mechanisms, and Management," *Environment International* 125 (2019): 365–385, https://doi.org/10.1016/J.ENVINT.2019.01.067.

16. T. Kemper and S. Sommer, "Estimate of Heavy Metal Contamination in Soils After a Mining Accident Using Reflectance Spectroscopy," *Environmental Science & Technology* 36, no. 12 (2002): 2742–2747, https://doi.org/10.1021/ES015747J.

17. H. Ha, J. R. Olson, L. Bian, and P. A. Rogerson, "Analysis of Heavy Metal Sources in Soil Using Kriging Interpolation on Principal Components," *Environmental Science & Technology* 48, no. 9 (2014): 4999–-5007, https://doi.org/10.1021/ES405083F.

18. S. K. Reza, U. Baruah, S. K. Singh, and T. H. Das, "Geostatistical and Multivariate Analysis of Soil Heavy Metal Contamination Near Coal Mining Area, Northeastern India," *Environmental Earth Sciences* 73, no. 9 (2015): 5425–5433, https://doi.org/10.1007/S12665-014-3797-1/METRICS.

19. G. Goncharov, B. Soktoev, I. Farkhutdinov, and I. Matveenko, "Heavy Metals in Urban Soil: Contamination Levels, Spatial Distribution and Human Health Risk Assessment (The Case of Ufa City, Russia)," *Environmental Research* 257 (2024): 119216, https://doi.org/10.1016/J.ENVRES.2024.119216.

20. A. Haghighizadeh, O. Rajabi, A. Nezarat, et al., "Comprehensive Analysis of Heavy Metal Soil Contamination in Mining Environments: Impacts, Monitoring Techniques, and Remediation Strategies," *Arabian Journal of Chemistry* 17, no. 6 (2024): 105777, https://doi.org/10.1016/J.ARABJC.2024.105777.

21. R. X. S. Tulcan, L. Liu, X. Lu, Z. Ge, D. Y. Fernández Rojas, and D. Mora Silva, "PAHs Contamination in Ports: Status, Sources and Risks," *Journal of Hazardous Materials* 475 (2024): 134937, https://doi.org/10.1016/J.JHAZMAT.2024.134937.

22. R Core Team, *R: The R Project for Statistical Computing* (R Core Team, 2025).

23. SEMARNAT, "Mexican Official Standard. NOM-021-RECNAT-2000: Especificaciones de fertilidad, Salinidad y Clasificación de Suelos," (2002), https://www.fao.org/faolex/results/details/es/c/LEX-FAOC050674/.

24. USEPA, *Method 9045D: Soil and Waste pH* (United States Environmental Protection Agency, 2004).

25. ISO, *ISO 11265: Soil Quality—Determination of the Specific Electrical Conductivity* (International Organization for Standardization, 1994).

26. USEPA, *EPA Method 3050B: Acid Digestion of Sediments, Sludges, and Soils* (US EPA, 1996).

27. L. Hakanson, "An Ecological Risk Index for Aquatic Pollution Control. A Sedimentological Approach," *Water Research* 14, no. 8 (1980): 975–1001, https://doi.org/10.1016/0043-1354(80)90143-8.

28. G. Muller, "Schwermetalle in den Sedimenten des Rheins Veranderungen seit 1971," *Umschau* 79 (1979): 778.

29. M. M. Hoque, A. Islam, A. R. M. T. Islam, S. C. Pal, S. Mahammad, and E. Alam, "Assessment of Soil Heavy Metal Pollution and Associated Ecological Risk of Agriculture Dominated Mid-Channel Bars in a Subtropical River Basin," *Scientific Reports* 13, no. 1 (2023): 11104, https://doi.org/10.1038/S41598-023-38058-0.

30. T. H. Hengl, *A Practical Guide to Geostatistical Mapping*, 2nd ed. (Publications Office of the European Union, 2009).

31. T. G. Pham, M. Kappas, C. V. Huynh, and L. H. K. Nguyen, "Application of Ordinary Kriging and Regression Kriging Method for Soil Properties Mapping in Hilly Region of Central Vietnam," *ISPRS International Journal of Geo-Information* 8 (2019): https://doi.org/10.3390/ijgi8030147.

32. A. Setiyoko, A. M. Arymurthy, and T. Basaruddin, "DEM Fusion Concept Based on the LS-SVM Cokriging Method," *International Journal of Image and Data Fusion* 10, no. 4 (2019): 244–262, https://doi.org/10.1080/19479832.2019.1664647.

33. E. Yalçin, "Cokriging and Its Effect on the Estimation Precision," *Journal of the South African Institute of Mining and Metallurgy* 105 (2005): 223–228.

34. A. Liu, C. Qu, J. Zhang, et al., "Screening and Optimization of Interpolation Methods for Mapping Soil-Borne Polychlorinated Biphenyls," *The Science of the Total Environment* 913 (2024): 169498, https://doi.org/10.1016/J.SCITOTENV.2023.169498.

35. D. Ccopi, E. Requena-Rojas, K. Ortega, R. Solórzano-Acosta, R. Révolo-Acevedo, and S. Pizarro, "Bioaccumulation of Heavy Metals in High Andean Crops of the Peruvian Andes: Comparative Evaluation Between Irrigated and Dry Systems," *Journal of Agriculture and Food Research* 25 (2025): 102575, https://doi.org/10.1016/J.JAFR.2025.102575.

36. I. W. Alejos-Patiño, H. Briceño-Yen, U. Campos-Felix, and J. Figueroa-Ramírez, "Evaluación de Metales Pesados en Suelo, Agua y Plantas Cultivadas en un Agroecosistema Periurbano de un Valle Interandino del Perú," *Bioagro* 38, no. 1 (2026): 509–522, https://doi.org/10.51372/bioagro381.10.

37. E. Tarrillo, M. Arce-Inga, P. A. Torres-Herrera, et al., "Geospatial Distribution of Heavy Metals in Rice Soils of Northwestern Peru," *Scientific Reports* 15, no. 1 (2025): 30692, https://doi.org/10.1038/s41598-025-16638-6.

38. F. Santos-Francés, A. Martínez-Graña, P. A. Rojo, and A. G. Sánchez, "Geochemical Background and Baseline Values Determination and Spatial Distribution of Heavy Metal Pollution in Soils of the Andes Mountain Range (Cajamarca-Huancavelica, Peru)," *International Journal of Environmental Research and Public Health* 14 (2017): 14, https://doi.org/10.3390/IJERPH14080859.

39. E. Orellana-Mendoza, M. Custodio, J. Ascensión, and M. C. Bastos, "Heavy Metals in Agriculture Soils From High Andean Zones and Potential Ecological Risk Assessment in Peru's Central Andes," *Journal of Ecological Engineering* 21, no. 8 (2020): 108–119, https://doi.org/10.12911/22998993/127094.

40. E. E. Golia, O. D. Kantzou, M. A. Chartodiplomenou, S. G. Papadimou, and N. G. Tsiropoulos, "Study of Potentially Toxic Metal Adsorption in a Polluted Acid and Alkaline Soil: Influence of Soil Properties and Levels of Metal Concentration," *Soil Systems* 7, no. 1 (2023): 16, https://doi.org/10.3390/soilsystems7010016.

41. S. D. Young, "Chemistry of Heavy Metals and Metalloids in Soils," in *Heavy Metals in Soils: Trace Metals and Metalloids in Soils and Their Bioavailability*, ed. B. J. Alloway (Dordrecht: Springer, 2013), 51–95.

42. T. Mitran, J. R. S. Gunnam, S. Gourigari, and S. Kandrika, "Assessment of Depth Wise Distribution, Enrichment, Contamination, Ecological Risk and Sources of Soil Heavy Metals Over an Industrial Area in Southern India," *Journal of Geochemical Exploration* 257 (2024): 107379, https://doi.org/10.1016/J.GEXPLO.2023.107379.

43. A. Kicińska, R. Pomykała, and M. Izquierdo-Diaz, "Changes in Soil pH and Mobility of Heavy Metals in Contaminated Soils," *European Journal of Soil Science* 73, no. 1 (2022): e13203, https://doi.org/10.1111/EJSS.13203.

44. M. Lian, Y. Ma, J. Li, J. Sun, and X. Zeng, "Influence of pH on the Particulate-Bound Cd Speciation and Uptake by Plants," *Polish Journal of Environmental Studies* 31, no. 6 (2022): 5511–5517, https://doi.org/10.15244/pjoes/152224.

45. S. Wierzba, J. Makuchowska-Fryc, A. Kłos, Z. Ziembik, and W. Ochędzan-Siodłak, "Role of Calcium Carbonate in the Process of Heavy Metal Biosorption From Solutions: Synergy of Metal Removal Mechanisms," *Scientific Reports* 12, no. 1 (2022): 17668, https://doi.org/10.1038/s41598-022-22603-4.

46. G. He, Z. Zhang, X. Wu, M. Cui, J. Zhang, and X. Huang, "Adsorption of Heavy Metals on Soil Collected From Lixisol of Typical Karst Areas in the Presence of $CaCO_3$ and Soil Clay and Their Competition Behavior," *Sustainability* 12, no. 18 (2020): 7315, https://doi.org/10.3390/SU12187315.

47. M. Graf, G. J. Lair, F. Zehetner, and M. H. Gerzabek, "Geochemical Fractions of Copper in Soil Chronosequences of Selected European Floodplains," *Environmental Pollution* 148, no. 3 (2007): 788–796, https://doi.org/10.1016/J.ENVPOL.2007.01.035.

48. S. N. Obasi, E. Jokthan G, C. Chinasa Obasi, and C. Onyeka Madueke, "Micronutrient Dynamics in Relation to Soil Properties in Arable Soils of Rigachikun-Kaduna, Northern Guinea Savannah, Nigeria," *Journal Clean WAS* 6, no. 1 (2022): 14–22, https://doi.org/10.26480/jcleanwas.01.2022.14.22.

49. M. Zhou, T. Hu, M. Wu, C. Ma, and C. Qi, "Rapid Estimation of Soil Mn Content by Machine Learning and Soil Spectra in Large-Scale," *Ecological Informatics* 81 (2024): 102615, https://doi.org/10.1016/J.ECOINF.2024.102615.

50. A. Elnajdi, A. Berland, J. Haeft, and C. Dowling, "Influence of Soil pH, Organic Matter, and Clay Content on Environmentally Available Lead in Soils: A Case Study in Muncie, Indiana, USA," *Open Journal of Soil Science* 13, no. 10 (2023): 414–430, https://doi.org/10.4236/ojss.2023.1310019.

51. J. J. González-Costa, M. J. Reigosa, J. M. Matías, and E. Fernández-Covelo, "Analysis of the Importance of Oxides and Clays in Cd, Cr, Cu, Ni, Pb and Zn Adsorption and Retention With Regression Trees," *PLoS One* 12, no. 1 (2017): e0168523, https://doi.org/10.1371/journal.pone.0168523.

52. Ministerio del Ambiente (MINAM), *Decreto Supremo NO 011-2017-MINAM* (Ministerio del Ambiente (MINAM), 2017).

53. Canadian Council of Ministers of the Environment (CCME), *Canadian Soil Quality Guidelines for the Protection of Environmental and Human Health: Zinc* (Canadian Council of Ministers of the Environment (CCME), 2018).

54. United States Environmental Protection Agency (USEPA), *Ecological Soil Screening Levels for Manganese* (United States Environmental Protection Agency (USEPA), 2007).

55. P. Makuleke and V. M. Ngole-Jeme, "Soil Heavy Metal Distribution With Depth Around a Closed Landfill and Their Uptake by *Datura stramonium*," *Applied and Environmental Soil Science* 2020 (2020): 8872475–14, https://doi.org/10.1155/2020/8872475.

56. J. O. Azeez, S. A. Mesele, B. O. Sarumi, J. A. Ogundele, A. O. Uponi, and A. O. Hassan, "Soil Metal Pollution as a Function of Traffic Density and Distance From Road in Emerging Cities: A Case Study of Abeokuta, Southwestern Nigeria," *Archives of Agronomy and Soil Science* 60, no. 2 (2014): 275–295, https://doi.org/10.1080/03650340.2013.792406.

57. T. Mdlambuzi, P. Muchaonyerwa, A. Mbangi, T. Mdlambuzi, P. Muchaonyerwa, and A. Mbangi, "Heavy Metals in Soils Following 50 Years of Sewage Sludge Application," in *Heavy Metals-Recent Advances* (London: IntechOpen, 2023), https://doi.org/10.5772/INTECHOPEN.110009.

58. Y.-B. Guo, H. Feng, C. Chen, C.-J. Jia, F. Xiong, and Y. Lu, "Heavy Metal Concentrations in Soil and Agricultural Products Near an Industrial District," *Polish Journal of Environmental Studies* 22 (2013): 1357–1362.

59. T. O. Kolawole, A. S. Olatunji, M. T. Jimoh, and O. T. Fajemila, "Heavy Metal Contamination and Ecological Risk Assessment in Soils and Sediments of an Industrial Area in Southwestern Nigeria," *Journal of Health and Pollution* 8, no. 19 (2019): 1–16, https://doi.org/10.5696/2156-9614-8.19.180906.

60. H. D. Weissmannová and J. Pavlovský, "Indices of Soil Contamination by Heavy Metals – Methodology of Calculation for Pollution Assessment (Minireview)," *Environmental Monitoring and Assessment* 189, no. 12 (2017): 616, https://doi.org/10.1007/s10661-017-6340-5.

61. L. P. Yiika, N. M. Jean-Lavenir, G. C. Suh, et al., "Distribution, Sources, and Eco-Toxicological Assessment of Potentially Toxic Metals in River Sediments of Nkwen Area (Cameroon Volcanic Line)," *Water, Air, & Soil Pollution* 235, no. 1 (2023): 16, https://doi.org/10.1007/S11270-023-06830-7.

62. N. A. Afahnwie, L. P. Yiika, C. S. Marian, et al., "Geospatial Distribution of Hazardous Metals and Other Elements in Stream Sediments of Akum, Cameroon: Insights Into Mineral Exploration and Ecosystem Health Using Indexical and Multivariate Approaches," *Marine Pollution Bulletin* 222 (2026): 118761, https://doi.org/10.1016/J.MARPOLBUL.2025.118761.

63. M. Saleem, D. Pierce, Y. Wang, D. A. Sens, S. Somji, and S. H. Garrett, "Heavy Metal(Oid)S Contamination and Potential Ecological Risk Assessment in Agricultural Soils," *Journal of Xenobiotics* 14, no. 2 (2024): 634–650, https://doi.org/10.3390/jox14020037.

64. M. Ximenes, J. A. M. S. Pratas, J. M. M. De Azevedo, and J. Ribeiro, "Evaluating the Concentration, Distribution, and Contamination of

Toxic Metals in the Urban Soil of Dili, Timor-Leste," *Geology, Ecology, and Landscapes* (2025): 1–22, https://doi.org/10.1080/24749508.2025.2535080.

65. E. Mouhsine, N. Ouazzani, M. Avila, and G. Perez, "Heavy Metal Contamination of Soils and Water Resources Kettara Abandoned Mine," *American Journal of Environmental Sciences* 8 (2012).

66. L. P. Yiika, M. A. Tita, C. E. Suh, M. E. Mimba, and N. M. Jean-Lavenir, "Heavy Metal Speciation by Tessier Sequential Extraction Applied to Artisanal Gold Mine Tailings in Eastern Cameroon," *Chemistry Africa* 6, no. 5 (2023): 2705–2723, https://doi.org/10.1007/S42250-023-00652-0.

67. A. Łukaszek-Chmielewska, J. Rakowska, M. Rachwał, and O. Stawarz, "Assessment of Forest Soil Contamination by Heavy Metals in the Polish National Park Near Warsaw," *Scientific Reports* 15, no. 1 (2025): 4099, https://doi.org/10.1038/s41598-025-88754-2.

68. O. I. Areguamen, P. Ekwumengbo, I. Omoniyi, et al., "Evaluation of the Source, Distribution and Risk of Metal Contaminated Stream Sediment," *Case Studies in Chemical and Environmental Engineering* 8 (2023): 100429, https://doi.org/10.1016/J.CSCEE.2023.100429.

69. Instituto Nacional de Estadística e Informática (INEI), *Sistema de Información Distrital para la Gestión Pública* (Instituto Nacional de Estadística e Informática (INEI), 2017).

70. A. F. Tiabou, G. A. A. Atabe, C. Sigue, L. P. Yiika, F. Kachoueiyan, and N. E. Forchenallah, "Appraisal of Pollution, Ecological and Health Risks Assessment of Trace Metals in Soils of Logbadjeck Quarrying Area, Nyong Series, Cameroon," *Journal of Trace Elements and Minerals* 10 (2024): 100204, https://doi.org/10.1016/J.JTEMIN.2024.100204.

71. Y. He, M. Luo, H. Yang, L. Bai, and Z. Chen, "Variability of Interpolation Errors and Mutual Enhancement of Different Interpolation Methods," *Applied Sciences* 14, no. 24 (2024): 11493, https://doi.org/10.3390/APP142411493.

72. D. Khodoli Zangeneh, H. Amanipoor, and S. Battaleb-Looie, "Evaluation of Heavy Metal Contamination Using Cokriging Geostatistical Method (Case Study of Abteymour Oilfield in Southern Iran)," *Applied Water Science* 13, no. 10 (2023): 200, https://doi.org/10.1007/s13201-023-01980-9.

73. M. Magno, I. Luffman, and A. Nandi, "Evaluating Spatial Regression-Informed Cokriging of Metals in Soils Near Abandoned Mines in Bumpus Cove, Tennessee, USA," *Geosciences* 11 (2021): 434, https://doi.org/10.3390/geosciences11110434.

74. J. Wu, W. A. Norvell, and R. M. Welch, "Kriging on Highly Skewed Data for DTPA-Extractable Soil Zn With Auxiliary Information for pH and Organic Carbon," *Geoderma* 134, no. 1-2 (2006): 187–199, https://doi.org/10.1016/J.GEODERMA.2005.11.002.

75. Y. Lv, G. Kabanda, Y. Chen, C. Wu, and W. Li, "Spatial Distribution and Ecological Risk Assessment of Heavy Metals in Manganese (Mn) Contaminated Site," *Frontiers in Environmental Science* 10 (2022): 942544, https://doi.org/10.3389/fenvs.2022.942544.

76. M. Alam, Z. Hussain, A. Khan, et al., "The Effects of Organic Amendments on Heavy Metals Bioavailability in Mine Impacted Soil and Associated Human Health Risk," *Scientia Horticulturae* 262 (2020): 109067, https://doi.org/10.1016/J.SCIENTA.2019.109067.

77. B. Wang, C. Wang, J. Li, H. Sun, and Z. Xu, "Remediation of Alkaline Soil With Heavy Metal Contamination Using Tourmaline as a Novel Amendment," *Journal of Environmental Chemical Engineering* 2, no. 3 (2014): 1281–1286, https://doi.org/10.1016/J.JECE.2014.05.017.

78. W. X. Ren, P. J. Li, Y. Geng, and X. J. Li, "Biological Leaching of Heavy Metals From a Contaminated Soil by *Aspergillus niger*," *Journal of Hazardous Materials* 167, no. 1–3 (2009): 164–169, https://doi.org/10.1016/J.JHAZMAT.2008.12.104.

79. S. A. Bhat, O. Bashir, S. A. Ul Haq, et al., "Phytoremediation of Heavy Metals in Soil and Water: An Eco-Friendly, Sustainable and Multidisciplinary Approach," *Chemosphere* 303 (2022): 134788, https://doi.org/10.1016/J.CHEMOSPHERE.2022.134788.

80. E. Elatafi, B. Elhendawy, S. Iqbal, et al., "Physicochemical, Metabolite, Osmolyte Synthesis, and Enzymatic Alterations of Grapevine Rootstocks in Response to Cadmium Stress," *Journal of Soil Science and Plant Nutrition* 2025 (2025): 1–19, https://doi.org/10.1007/S42729-025-02765-6.

81. N. Sun, F. Zhu, L. Sun, G. Zou, and H. Li, "Grafting on Rootstocks With Low Cd Accumulating Potential: A Green Technology in Vegetable Production," *Environmental Technology & Innovation* 38 (2025): 104077, https://doi.org/10.1016/J.ETI.2025.104077.

82. V. Lovynska, B. Bayat, R. Bol, et al., "Monitoring Heavy Metals and Metalloids in Soils and Vegetation by Remote Sensing: A Review," *Remote Sensing* 16, no. 17 (2024): 3221, https://doi.org/10.3390/RS16173221.